PHYSICAL REVIEW D

PARTICLES AND FIELDS

THIRD SERIES, VOLUME 33, NUMBER 9 1 MAY 1986

Observation of double phi-meson production in 400-GeV/c proton-nucleon interactions

T. F. Davenport,* J. R. Albright, J. H. Goldman, S. L. Hagopian, and J. E. Lannutti
Florida State University, Tallahassee, Florida 32306

K. W. Lai, J. LeBritton,† Y. C. Lin,‡ and A. E. Pifer
University of Arizona, Tucson, Arizona 85721

H. C. Fenker and D. R. Green
Fermilab, Batavia, Illinois 60510

G. E. Canough, C. C. Chang,§ T. C. Davis,** R. W. Joyner, and J. A. Poirier
University of Notre Dame, Notre Dame, Indiana 46556

C. H. Georgiopoulos†† and A. Napier
Tufts University, Medford, Massachusetts 02155

J. M. Marraffino, J. W. Waters, M. S. Webster, E. G. H. Williams,‡‡ and J. Woosley
Vanderbilt University, Nashville, Tennessee 37233

J. R. Ficenec, S. Torres,§§ and W. P. Trower
Virginia Polytechnic Institute and State University, Blacksburg, Virginia 24061
(Received 30 September 1985)

The production of ϕ-meson pairs has been observed in 400-GeV/c proton-nucleon interactions at the Fermilab multiparticle spectrometer in the inclusive reaction $pN \to \phi\phi + X$, where each ϕ decays to a K^+K^- pair. A fast (200 nsec) high-level processor was used to selectively trigger on events containing two pairs of oppositely charged kaons having low invariant masses. The experimental apparatus and trigger processor are described. The cross section for $\phi\phi$ production and an upper limit for η_c production are presented.

INTRODUCTION

The $\phi\phi$ decay channel has been suggested as a favorable place to look for hadronic production of glueballs,[1] the η_c, and exotic meson states having $C=+1$. Because of the narrow natural width of the ϕ, its large branching ratio into K^+K^- and the fact that inclusive kaon cross sections are much lower than pion cross sections in nucleon-nucleon reactions, background problems should be reduced relative to other final states such as $\rho\rho$ or $\omega\omega$. Also, the low Q value for the ϕ decay into K^+K^- tends to give a small opening angle in the laboratory, leading to good geometrical acceptance and the possibility of simple patterns for triggering purposes.[2]

This paper reports the results of Fermilab experiment E623, a particle search in the reaction

$$pN \to \phi\phi + X ,$$

where each ϕ decays to a K^+K^- pair. A fast trigger processor was used to trigger on events containing two K^+K^- candidate pairs, with each pair having a projected mass consistent with the ϕ mass. Approximately 3.6×10^6 triggers were recorded.

EXPERIMENTAL APPARATUS

The experiment was performed at the multiparticle spectrometer (FMPS) at the Fermi National Accelerator Laboratory (Fermilab). A beam of 400-GeV/c protons extracted from the main ring at Fermilab was directed onto the production target and diffracted protons were collimated and transported down the M6W beam line to the FMPS. The repetition rate of the beam was approxi-

mately 13 sec with each pulse lasting 1 sec. There were about 2×10^6 protons on target in each pulse.

The FMPS is a large, open-geometry spectrometer system designed to look at systems of charged particles in the forward direction. For this experiment the FMPS consisted of the following: 8 small multiwire proportional chambers (MWPC's) for beam tracking, a segmented scintillator target, 25 planes of MWPC's for tracking of secondary charged particles, a 0.6-m$\times$1.2-m$\times$1.2-m superconducting magnet (p_t kick$=$0.7 GeV/c) for momentum analysis, 2 multicell gas Cherenkov counters for particle identification, a scintillator hodoscope, 8 planes of 1.7-m $\times$3.3-m drift chambers used for tracking, and several small scintillator paddles used for triggering. The basic configuration can be seen in Fig. 1.

Using a 50% argon/ethane mixture, the resolution of the drift planes in our system ranged from about 280 to 600 μm. For both MWPC's and drift chambers the maximum rates that can be achieved are on the order of 10^6 events/sec due to the time required for the ions to be collected. For the drift chambers, the maximum drift time was about 200 nsec corresponding to the time required for an electron to drift across a half-cell (0.95 cm). The inverse saturated drift velocity was approximately 188 nsec/cm.

The MWPC's were grouped into eight stations where, in general, each station consisted of several sense planes. For example, the A station consisted of two x planes, two y planes, a u plane, and a v plane. Three of the stations were upstream of the target and were used for tracking the incident-beam particles. Stations A and B were located between the target and the magnet, station C was inside the magnet aperture, and stations D and F were downstream of the magnet. Signals from the wires were amplified by chamber-mounted preamplifiers with outputs connected to a set of shift registers. The shift registers received the signals from the wires in parallel, latched the inputs, and shifted the data out serially.

The drift-chamber planes were grouped into two stations DA and DB of four planes each and were located downstream of the magnet between MWPC stations D and F. Signals from the drift sense wires were amplified and discriminated at the chamber and then sent to a set of TDC's (time-to-digital converters). Since we used the common-stop mode for the TDC's, if there were two tracks in a single cell, we would only detect the last one to drift to the sense wire.

The target for the experiment consisted of 20 closely packed 3.175-cm$\times$3.175-cm$\times$0.635-cm scintillator segments with a total length of approximately 12.7 cm. The amount of material in the target corresponded to 0.20 inelastic interactions/beam particle (20% target). The purpose of the scintillator target was to help reduce multiple scattering effects relative to a thinner but more dense material. The pulse-height information from the phototubes gave an indication of the location of the primary interaction in the target.

Multicell threshold Cherenkov counters C_A and C_B

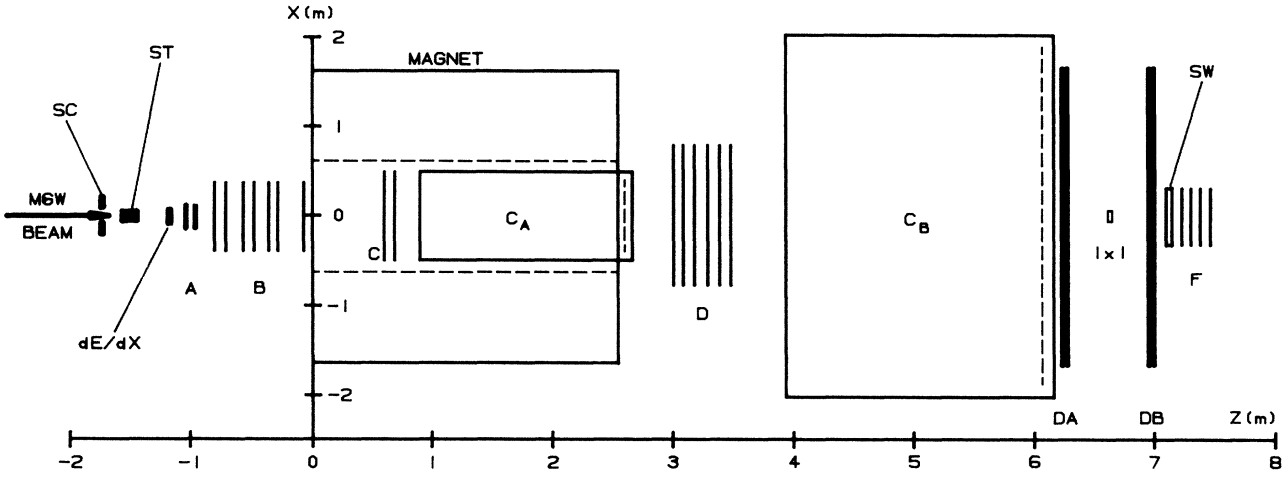

BEAM CHAMBERS

PWCe	Spacing	Planes
BA1	2 mm	Y X
BA2	2 mm	Y X V
BB	1 mm	X X Y

CHAMBER PARAMETERS

PWCe	Spacing	Planes	Wires
A	1 mm	X X1 Y Y1 U V	1536
B	2 mm	X Y X1 Y1 X2 Y2 U	2944
C	2 mm	X Y	832
D	2,3 mm	X Y U V Y1 X1	4416
F	2 mm	X Y U V	1280
Drift Chambers			
DA	19 mm	U V X1 X	736
DB	19 mm	U V X X1	736

FIG. 1. Experimental setup of Fermilab for E623.

were used for particle identification. Each cell in the counter is independent so that particles traversing different cells can be identified separately. Figures 2(a) and 2(b) show the mirror sizes and arrangements for C_A and C_B. Since C_A was inside the magnetic field it was not used for particle identification but only as a high pion multiplicity veto. Both C_A and C_B were filled with nitrogen gas at atmospheric pressure.

The scintillator hodoscope SW [Fig. 2(c)] was located just downstream of drift station DB and was designed to shadow the small angle mirrors of C_B. It was primarily used by the trigger processor to give vertical segmentation to the trigger hodoscope in the forward direction.

TRIGGER AND TRIGGER PROCESSOR

In order to look at processes with very small cross sections some method of distinguishing candidate events must exist. The trigger in this experiment performed this function by allowing only those events satisfying a set of predetermined conditions to be accepted and stored for later analysis.

The reaction that we are interested in is

$$pN \rightarrow \phi\phi + X \ ,$$

where each ϕ decays into a K^+K^- pair. Thus each event must have at least two K^+ tracks and two K^- tracks in order to be considered and, in addition, each K^+K^- pair must have low invariant mass. There are also the general requirements that the interaction take place in the target, the charged multiplicity not be too great, and the event not be too close in time to a previous event.

A good beam track was identified by using signals from three small scintillator counters SA, SB, and SC, located directly in front of the target. Counter SC was used to veto the accompanying beam halo. The condition for accepting a beam particle was given by

$$\mathrm{BM} = \mathrm{SA} \cdot \mathrm{SB} \cdot \overline{\mathrm{SC}} \ .$$

An interaction in the target was defined in two ways. The first used *dEdX*, a scintillator counter directly behind the target that gave a signal proportional to the number of charged particles passing through it. This allowed a multiplicity window requirement to be used. The second used 1×1, a 2.5-cm-by-2.5-cm scintillator counter located downstream of the magnet between drift stations DA and DB and directly in the path of the beam. The absence of a signal from 1×1 indicated that an interaction had occurred. The definition of a beam particle interacting in the target was then

$$\mathrm{IB} = \mathrm{BM} \cdot dEdX \geq 4 \cdot \overline{dEdX > 10} \cdot \overline{1\times1} \ .$$

Within 50 nsec of receiving an interacting beam signal, another signal, E (enable), was formed by requiring the number of cells having light in C_B to be less than five and the pulse height in *dEdX* to be less than 15, in units corresponding to that given by a single minimum ionizing particle, so that

$$E = \mathrm{IB} \cdot \overline{C_B > 5} \cdot \overline{dEdX > 15} \ .$$

The enable signal was used as a gate for the trigger pro-

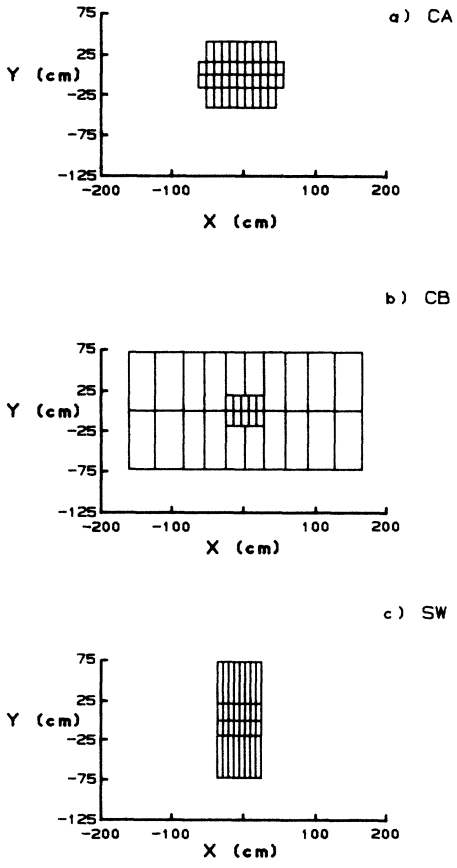

FIG. 2. (a) Cell segmentation for Cherenkov counter C_A. (b) Cell segmentation for Cherenkov counter C_B. (c) Scintillator wall segmentation.

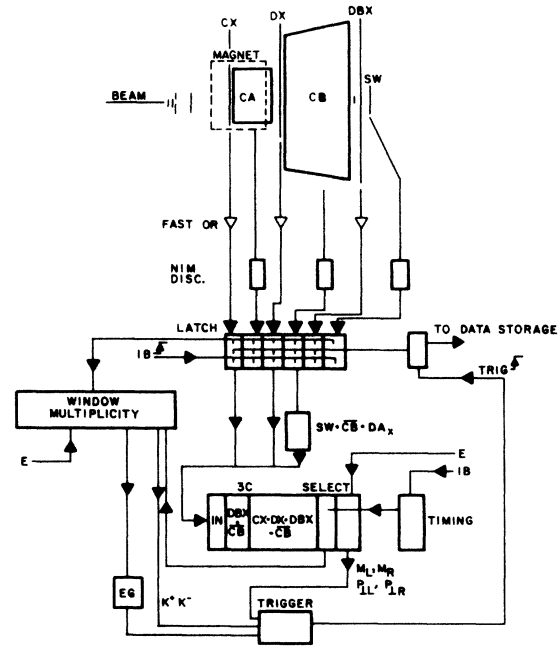

FIG. 3. Schematic diagram of trigger system.

cessor. If there was no enable the event was immediately aborted in order to reduce dead time.

The inputs to the trigger processor consisted of signals from C_A, C_B, and SW along with signals from wire-chamber planes CX, DX, and DBX, as shown in Fig. 3. The wire-chamber signals were combined with a logical OR at the chamber in order to form 32-element hodoscopes from each plane. The window discriminators produced a signal if the multiplicity N was between the limits $N_L \leq N < N_H$.

The outputs from the window discriminators were used to form another gate, EG (event gate), defined by

$$\mathrm{EG}=E\cdot\mathrm{CX}(4,10)\cdot\mathrm{DX}(4,10)\cdot\mathrm{DBX}(4,10)$$
$$\cdot\overline{C_A>8}\cdot\overline{C_B>6}\cdot\overline{\mathrm{SW}>7}\ .$$

This gate limited the total charged multiplicity. In addition, the multiplicities in C_A and C_B were required to agree within two.

A track was defined as a coincidental hit in all three elements of a predefined road through CX, DX, and DBX. A target point plus these three points provided redundant four-point tracking. Each road was uniquely identified by its x-z (magnet bend plane) production angle θ and momentum P. A track having no light in any C_B cells overlapping this road was defined to be kaon. The scintillator hodoscope SC was also used for tracks in the central region of C_B where there was a high particle density. The momentum range of the roads used by the trigger processor was between 6 and 22 GeV/c to match the gas mixture used in C_B. If several tracks of the same charge shared the same production angle only the highest-momentum track was reported to the higher-level trigger-processor logic.

The high-level logic of the trigger processor used the momenta and production angles of the kaon tracks to compute the effective mass of selected K^+K^- pairs. To emphasize high $\phi\phi$ effective masses the $\phi\phi$ trigger required two pairs with small opening angles between the K^+ and K^- in each pair and a large opening angle between the pairs. This was accomplished by choosing the pair of positive-kaon tracks K_L^+ and K_R^+ having the most positive and most negative production angle, respectively. The same was done for negative tracks K_L^- and K_R^-. The effective masses of the pairs $K_L^+K_L^-$ and $K_R^+K_R^-$ were then calculated from a memory look-up table using the approximation

$$(M_{K^+K^-})^2\simeq P_+P_-(\theta_+-\theta_-)^2\ ,$$

where P_+P_- and θ_+/θ_- were the projected momenta and production angles of the charged pair. If this was less than a Monte Carlo–determined cut, then the pair was accepted as a ϕ candidate and the M_L or M_R flag was enabled. For $\phi\phi$ triggers the requirement was

$$\phi\phi=\mathrm{EG}\cdot K^+(2,4)\cdot K^-(2,4)\cdot M_L\cdot M_R\ .$$

A schematic diagram of the trigger and trigger processor is shown in Fig. 3 and Table I gives the rates for the triggers used. A more extensive discussion of the trigger and especially the trigger-processor system and electronics can be found in Ref. 3.

TABLE I. Trigger rates.

Name	Trigger	σ (μb)
IB ($=\sigma_I$)		30 000
E		8 760
EG		1 077
$2K$	$\mathrm{EG}\cdot K^+(1,4)\cdot K^-(1,4)$	377
ϕ	$2K\cdot(M_L+M_R)$	121
$4K$	$\mathrm{EG}\cdot K^+(2,4)\cdot K^-(2,4)$	94
$2K\phi$	$4K\cdot(M_L+M_R)$	51
$\phi\phi$	$4K\cdot(M_L\cdot M_R)$	12

PARTICLE IDENTIFICATION

The Cherenkov counter C_B was filled with nitrogen gas at one atmosphere having an index of refraction $n=1.0003$. The calculated threshold momenta P_{thresh} for pions, kaons, and protons were 5.69, 20.15, and 38.30 GeV/c, respectively.

We find experimentally that the average number of photoelectrons detected by a phototube for a $\beta=1$ particle is approximately six, giving

$$N_{\mathrm{photoelectrons}}\simeq 6.0[1-(p_{\mathrm{thresh}}/p)^2]\ .$$

For particles of a given momentum the actual number of photoelectrons detected will be distributed according to a Poisson distribution. Figure 4 shows the average number of photoelectrons expected for pions, kaons, and protons of a given momentum in C_B.

For each track in the event, the Cherenkov cone in C_B was calculated as if the track were a pion. The intersection of the cone with the C_B mirrors was weighted to take into account the $1/r$ dependence of the distribution of photons in the cone. Next, the expected number of pho-

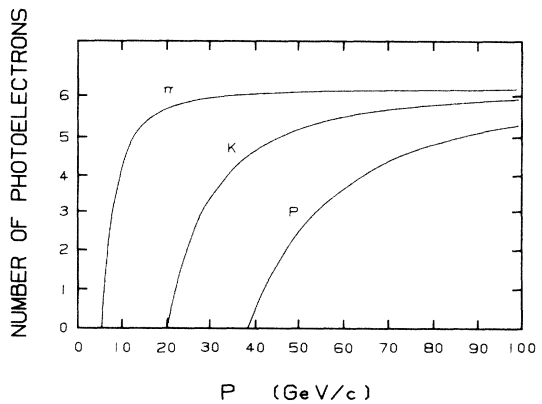

FIG. 4. Average number of photoelectrons expected in C_B for pions, kaons, and protons vs momentum.

toelectrons was calculated successively assuming the particle was a pion, kaon, or a proton using the formula discussed previously. All the weighted numbers of photoelectrons for the tracks were then stored by C_B mirror number and an expected pulse height was calculated for each mirror and mass assignment.

For mirrors with an observed pulse height below the one photoelectron cut, the tracks through each mirror were identified according to momentum. For a track to have been identified, it must have had at least 30% of its weighted area inside the mirror in question.

For mirrors with an observed pulse height above the one-photoelectron cut, the number of photoelectrons detected by the phototube was calculated. Then the tracks that had all or some of their Cherenkov cone in that mirror were examined. For tracks above proton threshold, assuming the track was either a pion, kaon, or proton, and after subtracting the expected signals, the identification was assigned that yielded the result closest to zero. If there were still photoelectrons left over, the same procedure was followed for tracks above the kaon threshold. If there were no photoelectrons left over, the tracks were assigned an identification according to their momentum. Otherwise the remaining photoelectrons were compared with the expected value for these tracks and a decision was made accordingly.

DATA SAMPLE

For this analysis, each event was required to have a vertex in the target and all tracks in the event were checked against each other for duplicate track parameters. If two tracks had the same upstream y slope within 0.3 mrad, the track with the lower quality was rejected.

Since we were looking for events with two ϕ mesons, each event was also required to have at least two identified K^+ and two identified K^- tracks with momentum above 5.8 GeV/c.

After making these cuts to the data as described previously there were a total of 122 430 events having at least two identified kaons of each charge type. All plots of E623 data in this paper were made from this sample.

DATA PRESENTATION AND ANALYSIS

The K^+K^- invariant-mass spectrum from threshold to 1.08 GeV/c^2 can be seen in Fig. 5. All possible K^+K^- combinations are included in the plot; for example, there would be four entries for an event with two kaons of each charge type. The ϕ resonance is clearly visible around 1.02 GeV. A fit to the spectrum was performed using a function of the form $Cx^{\alpha}(1-x)^{\beta}$, to represent the background, where C, α, and β were parameters to be varied and x was the rescaled mass defined to be between zero and one. The contribution from the ϕ resonance was fitted to a Gaussian distribution.

The value for the ϕ mass from the fit was 1.0197±0.0003 GeV, in good agreement with the accepted[4] value of 1.0196 GeV. The fitted value for σ (standard deviation of the Gaussian) was 4.3±0.4 MeV corresponding to a full width at half maximum (FWHM) of

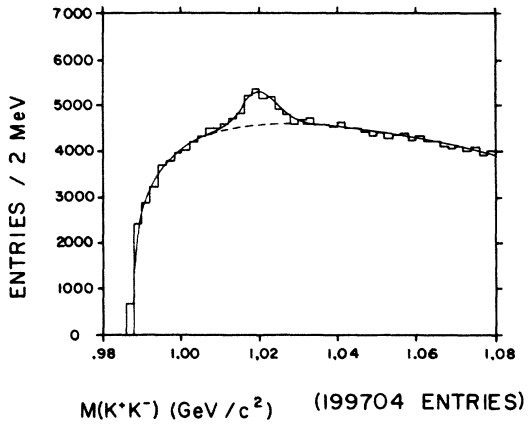

FIG. 5. K^+K^- invariant-mass spectrum.

10.1±0.9 MeV. This is much wider than the natural width[4] of the ϕ, but is consistent with a Monte Carlo–determined resolution.

Since each event has at least two K^+ and two K^- tracks we can make a plot of the other K^+K^- mass combination when the first one lies in the ϕ mass range, within ±6 MeV of the nominal ϕ mass. This spectrum is shown in Fig. 6. The second ϕ signal is clearly evident above the background, indicating that $\phi\phi$ production has been observed, although it should be noted that a true $\phi\phi$ event would have two entries in the plot.

A fit was done to the spectrum in Fig. 6 using the same form as before. The fitted value for the second ϕ mass was 1.0198±0.0005 GeV with a σ of 3.6±0.7 MeV corresponding to a FWHM of 8.4±1.6 MeV.

For the $\phi\phi$ mass spectrum, the mass of both K^+K^- combinations was required to be within ±6 MeV of the nominal ϕ mass. This spectrum is shown in Fig. 7. The spectrum rises sharply at threshold and falls exponentially beyond a mass of 2.20 GeV.

In order to estimate how much of this spectrum is true $\phi\phi$ production, as opposed to the background processes $K^+K^-K^+K^-$ and ϕK^+K^-, we use the two-dimensional

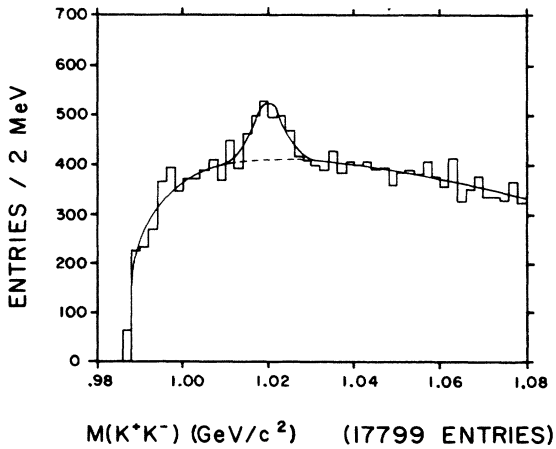

FIG. 6. K^+K^- invariant mass, cut on other ϕ mass (±6 MeV).

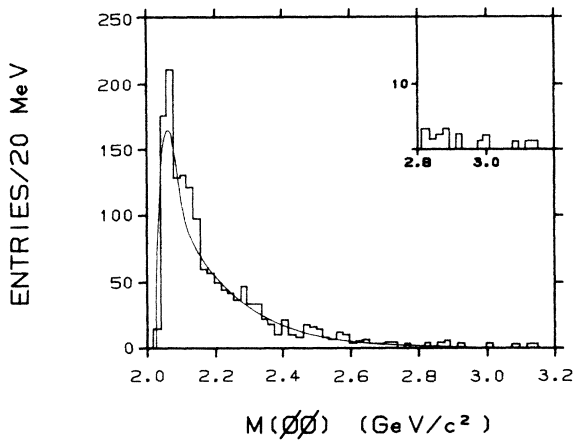

FIG. 7. $\phi\phi$ invariant-mass spectrum with fit to background regions.

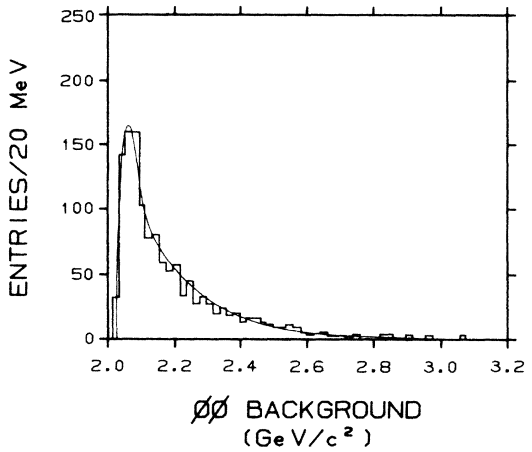

FIG. 9. Estimated $\phi\phi$ background spectrum and fitted curve.

plot of $M(K^+K^-)_1$ vs $M(K^+K^-)_2$. In Fig. 8(a) is shown the number of entries in the scatter plot summed over 12-MeV-by-12-MeV bins in the range 1.002—1.038 GeV. The central square is centered on the ϕ mass for each axis.

The plot is symmetric about the diagonal since each K^+K^- combination is entered twice in the plot, once as the first pair and then again as the second pair, and given a weight of 0.5 to avoid double counting.

We can estimate the background in the entire plot due to $K^+K^-K^+K^-$ production by looking at the four outside corners of the plot. Taking the average of these four squares and subtracting this from every square we have Fig. 8(b).

We next subtract the contribution to the $\phi\phi$ region from the two ϕK^+K^- bands. Averaging the four middle squares on the outside and subtracting (the $\phi\phi$ region has a double contribution) we have Fig. 8(c). All the bins in the plot are zero, within errors, except for the $\phi\phi$ bin which has a residual contribution above background of 177 ± 42 events. This number will be used later in the cross-section calculation for $\phi\phi$ production.

If we take the events in the background regions and normalize them according to the above procedure, we can plot the estimated $\phi\phi$ background spectrum. This spectrum was fit to a curve of the form $(M-M_0)^{\alpha_e-\beta(M-M_0)}$ and M_0, α, and β were fitted parameters. The background spectrum and the fitted curve are shown in Fig. 9 and the curve is also shown superimposed over the $\phi\phi$ spectrum in Fig. 7. The background-subtracted spectrum, in 20-MeV bins, is shown in Fig. 10. We see that the residual events in the spectrum are mainly concentrated at low $\phi\phi$ invariant mass. A discussion of the low-invariant-mass portion of this spectrum appears in Ref. 5.

a)

1.038	1085	1210	1114
1.026	1185	1474	1210
1.014	1110	1185	1085
1.002			

1.002 1.014 1.026 1.038 (GeV/c²)

M(K+K−)₁

M(K+K−)₂

b)

-13	112	16
87	376	112
12	87	-13

c)

-13	12	16
-12	177	12
12	-12	-13

FIG. 8. (a) Scatter plot of $M(K^+K^-)_1$ vs $M(K^+K^-)_2$. (b) After subtraction of $K^+K^-K^+K^-$ region. (c) After subtraction of $K^+K^-K^+K^-$ and ϕK^+K^- region.

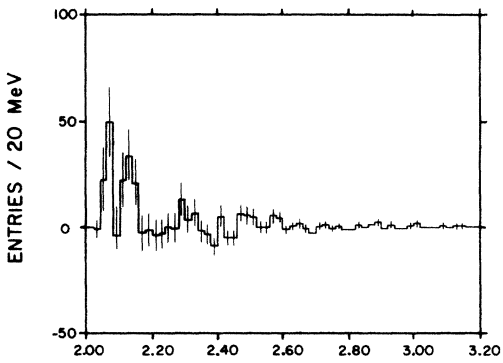

FIG. 10. $\phi\phi$ mass spectrum after background subtraction.

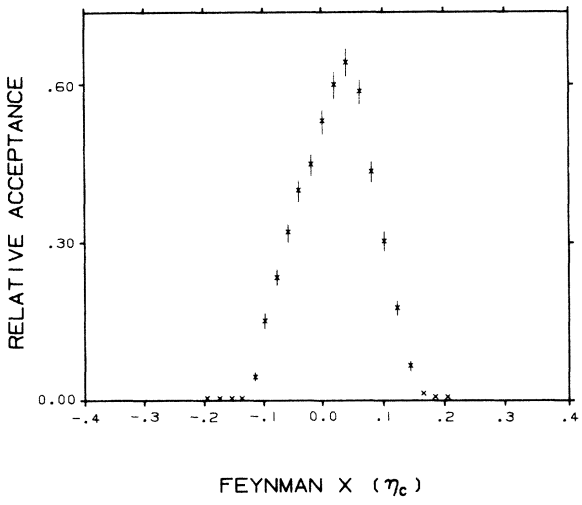

FIG. 11. Relative acceptance for $M(\phi\phi)=M(\eta_c)$ vs x_F.

RELATIVE ACCEPTANCE AND RESOLUTION

The experimental apparatus was configured so that the region of acceptance for $\phi\phi$ production as a function of x_F was confined to a rather narrow region ($|x_F| \leq 0.1$) centered about $x_F=0$. This was done because, for nucleon-nucleon interactions, the production of glueballs, the η_c and massive $s\bar{s}$ states is expected to take place primarily in the central region, $x_F \simeq 0$ (Refs. 6–8).

The most important factors in determining the limited range of x_F are the geometrical factors imposed by the spectrometer system and the momentum window for kaon identification imposed by the Cherenkov counter C_B. This information was used in a Monte Carlo program to calculate the relative acceptance. The ratio of the number of Monte Carlo events with all four kaons in the C_B momentum range and passing through the spectrometer, divided by the number of generated events was defined as the relative acceptance.

For $M(\phi\phi)=M(\eta_c)=2.98$ GeV/c^2, the relative acceptance as a function of x_F is shown in Fig. 11. The relative acceptance as a function of $\phi\phi$ invariant mass for three values of x_F is shown in Fig. 12. It is evident that, for $x_F \simeq 0$, the acceptance is reasonably flat over a wide range of $\phi\phi$ invariant masses.

The same Monte Carlo program was also used to determine the experimental resolution for observing a narrow state decaying to $\phi\phi$ as a function of mass. The Monte Carlo program was checked against the single-ϕ resolution which determines the scale of our resolution. The estimated $K^+K^-K^+K^-$ mass resolution (FWHM) as a function of mass is shown in Fig. 13. The two sets of points correspond to variances giving reconstructed ϕ widths of 8 and 10 MeV, giving an indication of the range of errors in the mass resolution.

ACCEPTANCE AND CROSS-SECTION CALCULATION

Since the actual production distributions for $\phi\phi$ are unknown, some type of model must be used to calculate the acceptance. For E623 the Lund Monte Carlo model[9] was used to generate typical, unbiased hadronic events.

The Lund model was used to generate a sample of events and a count was kept of the number of events generated as 1ϕ, 2ϕ, ϕK^+K^-, and so on. From this sample, only those events having at least one ϕ decaying to K^+K^- with both kaons in the Cherenkov momentum range ($5.7 < p_K < 23.0$) were kept for the rest of the analysis.

The four-vectors from the generated events were then used as input to another Monte Carlo program that simulated the Fermilab MPS. The simulation program propagated the particles through the spectrometer system, creating hits in the wire chambers and pulse heights in the analog-to-digital converters (ADC's) from the scintillators and Cherenkov phototubes. Realistic efficiencies and resolutions, estimated from our data, were used to describe all detectors. Multiple-scattering effects from material in the apparatus were also included. The gen-

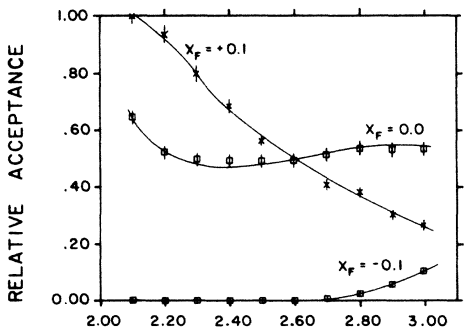

FIG. 12. Relative acceptance vs $M(\phi\phi)$ for $x_F=-0.1$, 0, 0.1.

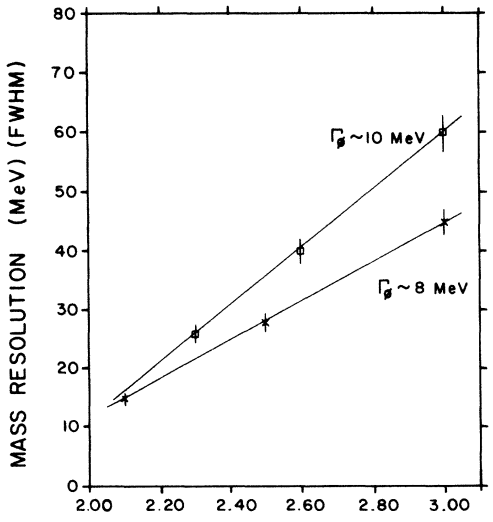

FIG. 13. Estimated mass resolution (FWHM) vs $M(K^+K^-K^+K^-)$.

erated information from the detectors was then used by a trigger-processor simulation program and those events that satisfied the trigger criteria were flagged. The output of the simulation program was written to tape in the same format as the raw data tapes for the experimental run. The Monte Carlo raw-data tapes were then processed by the same programs that were used for the actual data analysis and described previously.

For the $\phi\phi$ total cross section the acceptance was defined as the number of $\phi\phi$ events found by the processing programs divided by the total number of generated Monte Carlo events of that type. A correction factor of 1.61 was also required to account for the probability of any of the four charged kaons decaying in flight before reaching the Cherenkov counter C_B. Table II shows the numbers used for the acceptance and cross-section calculations.

The calculated value for the total inclusive $\phi\phi$ cross section at 400 GeV/c is 0.84 ± 0.27 μb per nucleon.

At the η_c mass we estimate that it would have required approximately six events over a background of three events in three 20-MeV bins to observe the η_c at the 99.7% confidence level (C.L.). Assuming that the acceptance for detecting the η_c is the same as for $\phi\phi$ and using the calculated sensitivity of approximately 5 nb per observed event, we arrive at an upper limit for

$$\sigma_T(pN\rightarrow\eta_c+X)B(\eta_c\rightarrow\phi\phi)\leq 30 \text{ nb} .$$

Using the measured η_c branching ratio[10] into $\phi\phi$ of $(8.0\pm2.5\pm2.0)\times10^{-3}$ we obtain a 99.7%-confidence-level upper limit for the cross section:

$$\sigma_T(pN\rightarrow\eta_c+X)\leq 3.75 \ \mu\text{b} .$$

TABLE II. Numbers used for $\phi\phi$ acceptance and cross-section calculation.

Total number of generated Monte Carlo events	56433
Total number of Monte Carlo events passing all cuts	24±4.9
Acceptance (%)	0.042±0.009
Correction factor for kaon decay	1.61
N_bN_t (events/nb) =(total live beam)× (number of target particle/cm^2)	800
Total number of observed events above background	177±42
Cross section (μb)	0.84±0.27

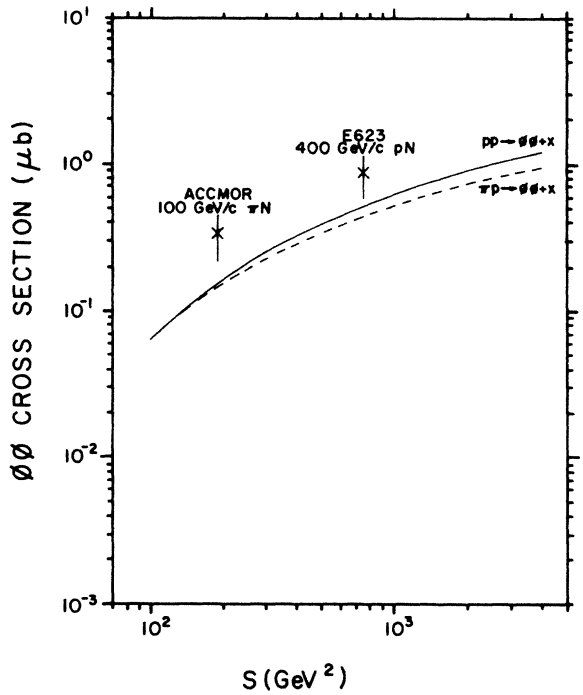

FIG. 14. $\phi\phi$ total-cross-section data and theoretical prediction using model of Li and Liu.

COMPARISON WITH THEORY

The measured inclusive $\phi\phi$ total cross section can be compared with a recent theoretical model given by Li and Liu.[11] They use a Drell-Yan-type mechanism with gluon fusion to produce a 2^{++} $s\,s\,\bar{s}\,\bar{s}$ state at 2.25 GeV/c^2 with a width of 360 MeV decaying predominantly to $\phi\phi$ that

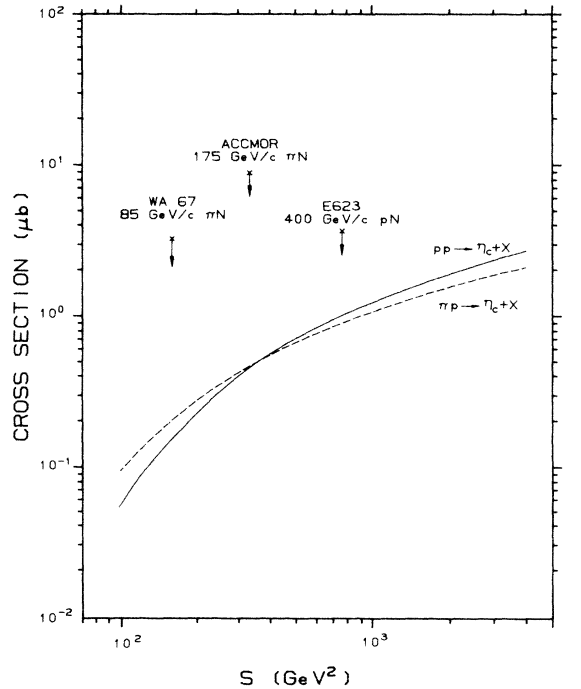

FIG. 15. Upper limits for η_c production and estimated η_c cross section using gluon-fusion model.

has been predicted according to the bag-model calculation of Jaffe.[12] Li and Liu assume that the 2^{++} state at 2.16 GeV/c^2 observed by Etkin *et al.*[13] is the state predicted by Jaffe and they use the measured mass and width in their calculation.

Their predictions for the $\phi\phi$ total cross section in πp and pp interactions versus s, are shown in Fig. 14 along with the data from E623 and the Amsterdam-Bristol-CERN-Cracow-Munich-Rutherford[14] (ACCMOR) Collaboration. Both experimental points are above the theoretical curves by a factor of about 1.5—2.0, but given the uncertainties of the model the agreement is reasonable.

The various upper limits available for η_c production[14,15] can be compared with the theoretical predictions for the η_c cross section using the gluon-fusion mode of Einhorn and Ellis.[7] The gluon distribution functions used in this case are those given by Duke and Owens[16,17] for pions and nucleons.

Figure 15 shows the experimental upper limits corrected for the η_c branching ratio into $\phi\phi$, along with the theoretical curves for πp and pp interactions. The upper limit for E623 at 3.75 μb is still about a factor of 4 above the predicted value, although it is the best limit to date in the sense of being the closest to the predicted curve. It appears that a much larger sample of high-energy inclusive $\phi\phi$ data would be needed to observe the η_c by this method.

CONCLUSIONS

We have observed inclusive production of ϕ-meson pairs in 400-GeV/c proton-nucleon interactions and measured the cross section to be 0.84 ± 0.27 μb/nucleon, and we obtain a 99.7%-C.L. upper limit for η_c production of 3.75 μb/nucleon.

ACKNOWLEDGMENTS

We would especially like to acknowledge the assistance provided by Rich Cantal and Sten Hansen of the FMPS group. This work was partially funded by the Department of Energy (Arizona, Fermilab, Florida State, Tufts) and the National Science Foundation (Arizona, Notre Dame, Vanderbilt, Virginia).

---

*Present address: Fermilab, Batavia, IL 60510.
†Present address: Burr-Brown Research Corp., Tucson, AZ 85706.
‡Present address: HEPL, Stanford, CA 94305.
§Present address: AT&T Laboratories, W. Long Beach, NJ 07764.
**Present address: AT&T Laboratories, Naperville, IL 60566.
††Present address: SCRI, Tallahassee, FL 32306.
‡‡Present address: 61 Batter Hall, Worchester, United Kingdom.
§§Present address: Lab. Nazionali, Frascatti (Roma) Italy.

[1]H. Lipkin, in *Experimental Meson Spectroscopy, 1977,* proceedings of the Vth International Conference, Boston, edited by E. von Goeler and R. Weinstein (Northeastern University Press, Boston, 1978).
[2]H. Lipkin, Report No. Fermilab-Conf-77/93-THY, 1977 (unpublished).
[3]H. Fenker *et al.*, Report No. Fermilab-Pub-82/62-EXP, 1982 (unpublished).
[4]Particle Data Group, Rev. Mod. Phys. **56**, S1 (1984).
[5]D. R. Green *et al.* Phys. Rev. Lett. (to be published).
[6]Y. Afek *et al.*, Nucl. Phys. **B165**, 339 (1980).
[7]M.E. Einhorn and S. D. Ellis, Phys. Rev. D **22**, 2007 (1975).
[8]S. R. Sharpe, Harvard University Report No. HUTP-84/A029, 1984 (unpublished).
[9]T. Sjostrand, Comput. Phys. Commun. **27**, 243 (1983).
[10]T. M. Baltrusaitis *et al.*, Phys. Rev. Lett. **52**, 2126 (1984).
[11]B. Li and K. Liu, Phys. Rev. D **28**, 1636 (1983).
[12]R. L. Jaffe, Phys. Rev. D **15**, 281 (1977).
[13]A. Etkin *et al.*, Phys. Rev. D **12**, 2007 (1982).
[14]C. Daum *et al.*, Phys. Lett. **104B**, 246 (1981).
[15]P. S. L. Booth *et al.*, Nucl. Phys. **B242**, 51 (1984).
[16]D. W. Duke and J. F. Owens, Phys. Rev. D **30**, 49 (1984).
[17]J. F. Owens, Phys. Rev. D **30**, 943 (1984).